Energy 79 (2015) 90–99

Contents lists available at ScienceDirect

Energy

journal homepage: www.elsevier.com/locate/energy

Development and analysis of a new renewable energy-based multi-generation system

Monu Malik [a, *], Ibrahim Dincer [a, b], Marc A. Rosen [a]

[a] Faculty of Engineering and Applied Science, University of Ontario Institute of Technology, 2000 Simcoe Street North, Oshawa, Ontario L1H 7K4, Canada
[b] Department of Mechanical Engineering, KFUPM, Dhahran 31261, Saudi Arabia

ARTICLE INFO

Article history:
Received 20 January 2014
Received in revised form
5 July 2014
Accepted 21 October 2014
Available online 5 December 2014

Keywords:
Renewable energy
Exergy
Energy
Efficiency
Geothermal
Biomass

ABSTRACT

A renewable energy-based multi-generation system is developed and studied energetically and exergetically. Two renewable sources of energy, biomass and geothermal, are combined to deliver five useful outputs for residential applications. The energy products from biomass sources are used to drive an organic Rankine cycle and a vapour absorption chiller, and further used to dry the wet material in an industrial dryer. A double flash system is used in the geothermal power cycle, which includes a multi-stage steam turbine. Outlet water flows from the separators and the steam turbine are used to heat water used in households. Liquefied gas is produced through the Linde Hampson liquefaction cycle, in which the compressor is directly coupled to organic Rankine cycle turbine. The energy efficiency of the system is found to be 56.5% and the exergy efficiency 20.3%. The largest exergy destructions are found to occur in both combustion chamber and boiler. The variations in exergy efficiencies and exergy destructions for the system components are determined with respect to changes in the reference-environment temperature and other major system parameters.

© 2014 Elsevier Ltd. All rights reserved.

1. Introduction

Energy plays an important role in the development of a country. With increases in world population and living standards, world energy demand is increasing steadily. But fossil fuel reserves are limited. The oil price shocks in the mid-1970s hastened the search for alternative energy sources like renewable energy, which can help overcome energy challenges. These efforts have continued since then, as have efforts to improve the efficiencies of energy systems.

Numerous renewable energy sources are available in nature like solar, biomass, hydro, wind, wave, tidal, ocean current, ocean thermal, and geothermal. Geothermal energy is an environmentally benign and sustainable energy source, as pointed out by Murphy et al. [1], Gunerhan et al. [2] and others. Ozgener et al. [3] have investigated geothermal energy applications such as electricity generation, heating, cooling and drying; these vary depending on the geothermal source temperature. Coskun et al. [4] performed an exergoeconomic analysis of geothermal power plants. Recently much research has been reported on biomass as a renewable source of energy (e.g., Dincer et al. [5]). Biomass is biological material from living matter on Earth, and can either be used directly as energy or converted into other energy products such as biofuels. Filho et al. [6] point out that biomass energy is used for such applications as heating, cooling and electricity production. Al-Sulaiman et al. [7] carried out energy and exergy analyses of an organic Rankine cycle driven by biomass.

To shift towards sustainability, it is important to utilize energy resources efficiently, in terms of avoiding external waste emissions and irreversibilities. In single generation (or product) cycles, there are always some losses due to thermal energy dissipation, e.g. exhaust gases from a gas turbine. In order to increase the efficiency of a system, such waste energy can be utilized for useful purposes (space or water heating, cooling using absorption chillers, industrial drying, etc.). Multi-generation is one approach to increasing the efficiency of energy systems and, as described by Dincer et al. [8,9], the combination of multi-generation and renewable energy systems can provide significant benefits. A multi-generation energy system produces, from one or more primary energy inputs, several useful outputs (e.g., electricity, heating, cooling, drying and gas liquefaction) according to Pouria et al. [10]. Zamfirescu et al. [11] demonstrated that the energy efficiency of a concentrated solar power system can be increased from 15 to 80% through cogeneration by recovering the heat which is normally rejected by the

* Corresponding author.
E-mail addresses: monu.malik@uoit.ca (M. Malik), ibrahim.dincer@uoit.ca (I. Dincer), marc.rosen@uoit.ca (M.A. Rosen).

http://dx.doi.org/10.1016/j.energy.2014.10.057
0360-5442/© 2014 Elsevier Ltd. All rights reserved.

Nomenclature

ex	specific exergy (kJ/kg)
$\dot{E}x$	exergy rate (kW)
$\dot{E}x^{Q}$	thermal exergy rate (kW)
h	specific enthalpy (kJ/kg)
LHV	lower heating value (kJ/kg)
$\dot{m}$	mass flow rate (kg/s)
M_u	moisture content in biomass (%)
P	pressure (kPa)
$\dot{Q}$	heat transfer rate (kW)
R	gas constant (kJ/kg K)
s	specific entropy (kJ/kg K)
T	temperature (K)
v	specific volume (m^3/kg)
w,a,b,c	stoichiometric constant in biomass combustion reaction in Eq. (1) (moles)
$\dot{W}$	work rate (kW)
x_k	number of molecules of gas k (molecules)
y,z	constant in Eq. (2) related to number of atoms of hydrogen and oxygen in biomass

Greek letters

η	energy efficiency
Ψ	exergy efficiency
Φ	exergy-to-energy ratio of fuel
μ_m	mineral matter content in biomass
λ	stoichiometric constant in biomass combustion reaction in Eq. (1) (moles)
$\alpha,\beta,\delta,\gamma$	number of atoms of carbon, hydrogen, nitrogen and oxygen in biomass (atoms/mole)

Subscripts

ACS	absorption chiller system
c	compressor
cc	combustion chamber
ch	chemical
d	destruction
dry	dry with no moisture content
e	evaporator
en	energetic
ex	exergetic
f	fuel
gen	absorption generator
geo	geothermal
HE	heat exchanger
l	loss
liq	liquefaction
mois	moisture
mg	multi-generation
o	overall
ORC	organic Rankine cycle
p	pump
ph	physical
s	source
sg	single generation
T	turbine
TIT	turbine inlet temperature
x,y,z	number of atoms of carbon, hydrogen and oxygen in biomass (atoms/molecule)
0	ambient (or reference-environment) condition
1 … 47	state numbers

thermal cycle. Bhattacharyya and Thuy [12] similarly assessed a cogeneration system for power and heat for the pulp and paper industry. Al-Sulaiman et al. [13] investigated a multi-generation system that integrates a SOFC (solid oxide fuel cell) with an organic Rankine cycle to generate electricity and an absorption chiller for cooling. Using exergy analysis, Dincer et al. [14] showed for a cogeneration system that integrates a gas turbine with a SOFC that cogeneration raises the overall energy efficiency to 66%. These studies show that multi-generation often has the potential to increase system efficiency.

The LH (Linde Hampson) cycle is a well-known cryogenic cycle for gas liquefaction and has been used for various purposes. Wiegerinck et al. [15] used the Linde Hampson cold stage in a sorption compressor cell with a single sorber bed, whereas Maytal [16] optimized the mass flow rate in order to maximize the rate of production of a liquid cryogen. In a study, Kanoglu et al. [17] used the LH cycle for the liquefaction of hydrogen gas using geothermal energy. Presently, however, hybrid membrane/cryogenic separation through cryogenic distillation is commonly employed [18].

The organic Rankine cycle is most common cycle used for low and medium temperature applications. Carcasci et al. [19] used the organic Rankine cycle for waste heat recovery from gas turbines and perform a thermodynamic analysis. In another study, Calise et al. [20] carried out a thermo-economic analysis and performance assessment of an organic Rankine cycle driven by medium temperature heat sources. Numerous types of fluids can be used as the working fluid in an organic Rankine cycle, one of the most common being n-octane due to its various advantages. Markus et al. [21] utilized n-octane in a double-stage biomass fired organic Rankine cycle for micro-cogeneration and provide a list of potential high-temperature circuit working fluids.

In the present paper, a new renewable energy-based multi-generation system is developed and assessed based on energy and exergy analyses. The present system employs two renewable energy inputs (e.g., biomass and geothermal) and yields five outputs (e.g., electricity, hot water, cooling, liquefied gas and heated drying air). The parametric studies are conducted to investigate the effects varying operating conditions and state properties on the system performance. Another objective of this study is to improve understanding of such integrated systems for multi-generation purposes.

2. System description

The multi-generation system considered here (see Fig. 1) consists of a biomass combustion cycle, an ORC (organic Rankine cycle), an absorption chiller cycle, a Linde Hampson liquefaction cycle, a geothermal power plant, a water heating system and a dryer. Biomass and geothermal water are the primary energy inputs, but the energy sources are combined so that the ORC output heat warms the incoming saturated water from the geothermal well.

At points 16 and 17 in Fig. 1, biomass and air respectively, at a specified air fuel ratio, enter a high-temperature combustion chamber. The high-temperature combustion gas exits the chamber at point 18, and passes through a cyclone where ash is removed. At the exit of cyclone at point 19 the combustion gas enters the boiler where heat is transferred from it to an organic fluid (n-octane). The combustion gas exits the boiler at a comparatively low temperature

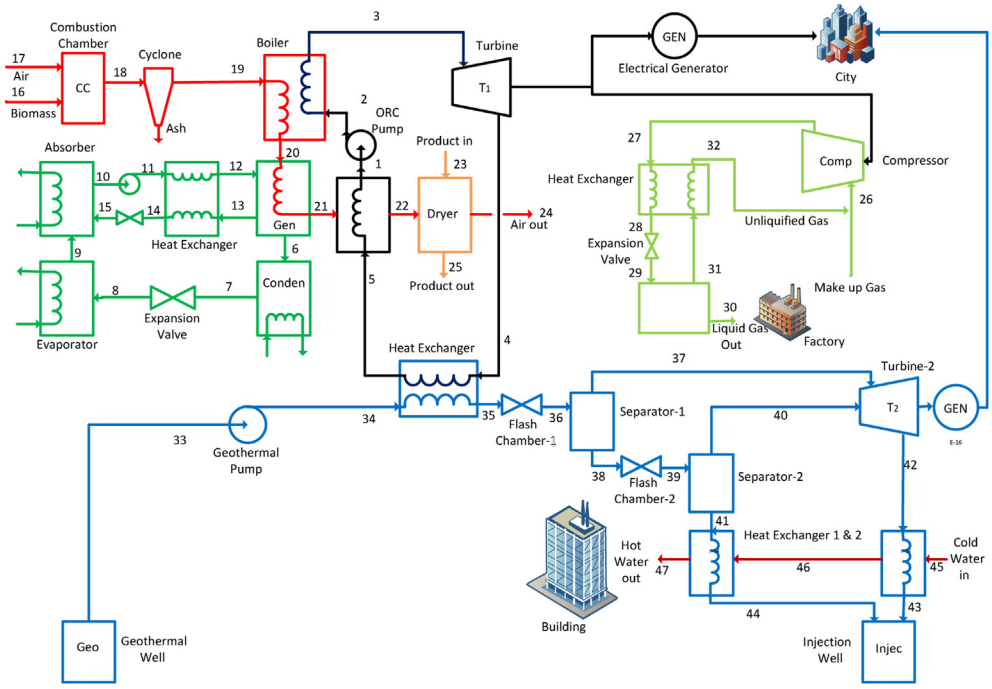

Fig. 1. Layout of the developed multi-generation system. Note that the Linde Hampson liquefaction cycle is utilized in the present study, even though it is not very common nowadays. The system aims to provide option for practical applications. A modern cryogenic cycle can be used in the future for better efficiency.

at point 20, and then enters the generator of an absorption chiller, where heat is transferred to the LiBr – H_2O solution. Then the low temperature combustion gas is heated by the ORC fluid (n-octane) in a heat exchanger between points 21 and 5, and enters a dryer at medium temperature, where it is used to reduce the moisture content of wet product (e.g. wheat). Finally, the combustion gas exits to the atmosphere at point 24 at low temperature and with high relative humidity.

The heat transferred by combustion gas between points 20 and 21 to the absorption chiller generator increases the temperature of the LiBr – H_2O solution, shifting part of the solution to water vapour. The water vapour enters a condenser at point 6 and is converted again to water after transferring heat to a cooling source. The water then exits the condenser at point 7 in a liquid state and passes through an expansion valve where its pressure and temperature drop. The chilled water enters the evaporator at point 8 and after absorbing heat from the cooling load of the building, converting it to a vapour, which exits the evaporator at point 9. The vapour next passes through the absorber (where it mixes with the strong solution of LiBr – H_2O from the absorption chiller generator), a heat exchanger and an expansion valve at points 13, 14 and 15, respectively. After mixing, a weak solution of LiBr – H_2O exits and is pumped to the absorption chiller generator through a heat exchanger between points 10 to 12.

In the boiler, heat is transferred from hot combustion gas from the combustion chamber to the ORC working fluid. This fluid at high-temperature and pressure enters the ORC turbine at point 3 and leaves at low pressure and medium temperature. The turbine exhaust is used to heat the incoming geothermal water via a heat exchanger between points 4 and 5 and then to heat the combustion gas from the absorption chiller generator between points 1 and 5 via another heat exchanger. The organic fluid n-octane as a liquid at point 1 is pumped to the boiler pressure and receives heat from the hot combustion gas. Part of turbine output drives the compressor used in the Linde Hampson liquefaction cycle and the remainder is converted to electricity via a generator.

In the Linde Hampson liquefaction cycle, a gas (air) enters the compressor at ambient temperature at point 26 and is compressed isothermally to a high pressure. It enters a heat exchanger at point 27, where the gas is cooled with the gas (not yet liquefied) entering the heat exchanger at point 31. Then the gas expands isenthalpically in the expansion valve between points 28 and 29, and a fraction of it is converted to liquid state and collected at point 30. The remainder in gaseous form at low temperature is passed to the compressor at point 28 through a heat exchanger. The compressor drive is coupled with the turbine in order to avoid the mechanical-to-electricity and electricity-to-mechanical conversion losses, as shown in Fig. 1.

The compressed hot water from the geothermal well at point 33 is further pressurized with a pump and then conveyed through a heat exchanger at point 34, where it gains heat from the ORC turbine exhaust. A double flash system is used to increase the mass flow rate of steam. Hot saturated water expands isenthalpically at points 35 and 38. Steam is separated from the water in separators 1 and 2 at points 36 and 39 respectively. The two steam flows enter a two-stage steam turbine at different conditions at points 37 and 40. The remaining water from separator 2 and the exhaust saturated vapour from the turbine are used to further heat the water at points 41 and 42 via heat exchangers 1 and 2, at points 45 and 46. The shaft work output of the steam turbine is converted to electricity in a generator. The hot water at point 47 is used in the residential building.

3. Energy and exergy analyses

To analyze the system, mass, energy, entropy and exergy balances are written for each component. The reference-environment temperature T_0 and pressure P_0 are taken to be 298 K and 101.325 kPa, respectively, reflecting the ambient conditions. Energy and exergy efficiencies are defined for major components and COPs (coefficients of performance) are expressed for the absorption

chiller and the Linde Hampson liquefaction cycle. Several assumptions are made for the present analysis:

- The heat losses through the pipes are negligible, whereas the heat losses from the turbines, combustion chamber and heat exchangers are considered for analysis.
- The isentropic efficiencies of all pumps, compressors and turbines are taken to be 85%, based on typical devices [22].
- The changes in kinetic and potential energies are negligible throughout the system.
- The hot water from the geothermal well is pressurized.
- The mass losses from the cyclone and other points in the system are negligible.

3.1. Biomass processes

As shown in Fig. 1, biomass fuel at point 16 and air at point 17 both enter the combustion chamber. The biomass combustion reaction, for a general biomass composition, is expressed as follows:

$$C_xH_yO_z + w\,H_2O + \lambda(O_2 + 3.76\,N_2) \rightarrow a CO_2 + b H_2O + c N_2 \tag{1}$$

The biomass chemical composition is determined with the method of Pouria et al. [23], where x, y and z are number of atoms of carbon, hydrogen and oxygen, respectively after the normalization. To find the physical exergy of the fuel, its lower heating value is determined as.

$$\overline{\mathrm{LHV}}_{\mathrm{dry}} = \frac{400,000 + 100,600y - \left(\frac{z}{1+0.5y}\right)(117,600 + 100,600y)}{12 + y + 16z} \tag{2}$$

which is applicable when number of atom of carbon in biomass chemical composition is unity after normalization.

The biomass in general contains some moisture, which affects its LHV (lower heating value) as follows [24]:

$$\overline{\mathrm{LHV}}_{\mathrm{mois}} = \left(1 - \mu_{\mathrm{m}} - M_{\mathrm{u}}\right)\overline{\mathrm{LHV}}_{\mathrm{dry}} - 2500 M_{\mathrm{u}} \tag{3}$$

where μ_{m} and M_{u} are the mineral matter content and the moisture content of the biomass, respectively.

To determine the chemical exergy of fuels, the exergy-to-energy ratio is employed as

$$\Phi = \frac{\mathrm{ex_f}}{\mathrm{LHV}} \tag{4}$$

For a substance with chemical formula $C_\alpha H_\beta N_\gamma O_\delta$, Φ can be calculated from the relation of Szargut et al. [25]:

$$\Phi = 1.0401 + 0.1728\frac{\beta}{\alpha} + 0.0432\frac{\delta}{\alpha} + 0.2169\frac{\gamma}{\alpha}\left(1 - 2.062\frac{\beta}{\alpha}\right) \tag{5}$$

The specific physical and chemical exergies of the fuel before and after combustion are calculate as described by Dincer et al. [26]:

$$\overline{\mathrm{ex}}_{\mathrm{ch}} = \sum x_{\mathrm{k}}\overline{\mathrm{ex}}^{\mathrm{k}}_{\mathrm{ch}} + RT_0\sum x_{\mathrm{k}}\ln(x_{\mathrm{k}}) \tag{6}$$

$$\overline{\mathrm{ex}}_{\mathrm{ph}} = (h_{\mathrm{k}} - h_0) - T_0(s_{\mathrm{k}} - s_0) \tag{7}$$

The mass and energy rate balances respectively for the combustion chamber can be written as

$$\dot{m}_{16} + \dot{m}_{17} = \dot{m}_{18} \tag{8}$$

$$\dot{m}_{16}h_{16} + \dot{m}_{17}h_{17} = \dot{m}_{18}h_{18} + \dot{Q}_{\mathrm{l_{cc}}} \tag{9}$$

The exergy destruction rate for the combustion chamber can be expressed as

$$\dot{m}_{16}\mathrm{ex}_{16} + \dot{m}_{17}\mathrm{ex}_{17} = \dot{m}_{18}\mathrm{ex}_{18} + \dot{Q}_{\mathrm{l_{cc}}}\left(1 - \frac{T_0}{T_{\mathrm{s,cc}}}\right) + \dot{\mathrm{E}}\mathrm{x}_{\mathrm{d}}^{\mathrm{cc}} \tag{10}$$

An energy rate balance for the boiler can be written as

$$\dot{m}_{19}h_{19} + \dot{m}_2h_2 = \dot{m}_{20}h_{20} + \dot{m}_3h_3 + \dot{Q}_{\mathrm{l_{boiler}}} \tag{11}$$

The exergy destruction rate for the boiler can be determined as

$$\dot{m}_{19}\mathrm{ex}_{19} + \dot{m}_2\mathrm{ex}_2 = \dot{m}_{20}\mathrm{ex}_{20} + \dot{m}_3\mathrm{ex}_3 + \dot{Q}_{\mathrm{l_{boiler}}}\left(1 - \frac{T_0}{T_{\mathrm{s,boiler}}}\right) + \dot{\mathrm{E}}\mathrm{x}_{\mathrm{d}}^{\mathrm{boiler}} \tag{12}$$

3.2. Organic Rankine cycle

The energy and exergy balances for the ORC turbine can be written respectively as

$$\dot{m}_3h_3 = \dot{m}_4h_4 + \dot{W}_{\mathrm{T_{ORC}}} \tag{13}$$

$$\dot{m}_3\mathrm{ex}_3 = \dot{m}_4\mathrm{ex}_4 + \dot{W}_{\mathrm{T_{ORC}}} + \dot{\mathrm{E}}\mathrm{x}_{\mathrm{d}}^{\mathrm{T_{ORC}}} \tag{14}$$

The work rate done by the ORC pump can be expressed as

$$\dot{W}_{\mathrm{p}} = \dot{m}_1v_1(P_2 - P_1) \tag{15}$$

where v_1 is the specific volume of water at point 1, and P_1 and P_2 are the pressures at points 1 and 2, respectively.

The ORC turbine exhaust is used to heat the geothermal water in a heat exchanger, for which an energy rate balance can be written as follows:

$$\dot{m}_4h_4 + \dot{m}_{34}h_{34} = \dot{m}_5h_5 + \dot{m}_{35}h_{35} + \dot{Q}_{\mathrm{l_{HE}}} \tag{16}$$

The exergy destruction rate for the heat exchanger is calculated as

$$\dot{m}_4\mathrm{ex}_4 + \dot{m}_{33}\mathrm{ex}_{33} = \dot{m}_5\mathrm{ex}_5 + \dot{m}_{34}\mathrm{ex}_{34} + \dot{Q}_{\mathrm{l_{HE}}}\left(1 - \frac{T_0}{T_{\mathrm{s,HE}}}\right) + \dot{\mathrm{E}}\mathrm{x}_{\mathrm{d}}^{\mathrm{HE}} \tag{17}$$

3.3. Absorption chiller

For the absorption chiller, the energetic COP can be expressed as

$$\mathrm{COP}_{\mathrm{en,ACS}} = \frac{\dot{m}_8(h_9 - h_8)}{\dot{m}_{20}(h_{20} - h_{21})} \tag{18}$$

and the exergetic COP as

$$\mathrm{COP}_{\mathrm{ex,ACS}} = \frac{\dot{m}_8(h_9 - h_8)\left(1 - \frac{T_0}{T_{\mathrm{se}}}\right)}{\dot{m}_{20}(h_{20} - h_{21})\left(1 - \frac{T_0}{T_{\mathrm{sgen}}}\right)} \tag{19}$$

3.4. Linde Hampson liquefaction cycle

Assuming that air behaves as an ideal gas during this isothermal compression process, the power required by liquefaction cycle compressor, which is coupled with the ORC turbine, can be written as:

$$\dot{W}_c = \dot{m}_{26}\, RT_{27} \ln \frac{P_{27}}{P_{26}} \tag{20}$$

where R is the gas constant.

The heat loss during isothermal compression can be determined from an energy rate balance as

$$\dot{m}_{26}h_{26} + \dot{W}_c = \dot{m}_{27}h_{27} + \dot{Q}_{l_c} \tag{21}$$

The exergy destruction rate for the compressor can be calculated as

$$\dot{m}_{26}ex_{26} + \dot{W}_c = \dot{m}_{27}ex_{27} + \dot{Q}_{l_c}\left(1 - \frac{T_0}{T_{s,c}}\right) + \dot{E}x_d^c \tag{22}$$

The COP of the liquefaction cycle can be calculated as the ratio of the heat rejected to the surroundings at the compressor to the work input to the compressor [26] as follows:

$$COP_{en,liq} = \frac{(h_{26} - h_{27})}{(h_{27} - h_{26}) - T_{27}(s_{27} - s_{26})} \tag{23}$$

3.5. Geothermal power cycle

The work input rate to the geothermal pump, which pumps water from the geothermal well to the heat exchanger and increases the pressure of the hot water, can be written as

$$\dot{W}_p = \dot{m}_{33}v_{33}(P_{34} - P_{33}) \tag{24}$$

where v_{33} is the specific volume of water at point 33, and P_{33} and P_{34} are the pressures at points 33 and 34.

The enthalpies of the flows remain constant across the flash chambers, so for Flash Chambers 1 and 2 the following can be written:

$$h_{35} = h_{36} \text{ and } h_{38} = h_{39} \tag{25}$$

For separators 1 and 2, where steam is separated from water, energy rate balances can be written, accounting for the assumption that heat losses are negligible, as follows:

$$\dot{m}_{36}h_{36} = \dot{m}_{37}h_{37} + \dot{m}_{38}h_{38} \quad \text{and} \quad \dot{m}_{39}h_{39} = \dot{m}_{40}h_{40} + \dot{m}_{41}h_{41} \tag{26}$$

The energy and exergy rate balances respectively can be written for the two-stage steam turbine as

$$\dot{m}_{37}h_{37} + \dot{m}_{40}h_{40} = \dot{m}_{43}h_{43} + \dot{W}_{T_{steam}} \tag{27}$$

$$\dot{m}_{37}ex_{37} + \dot{m}_{40}ex_{40} = \dot{m}_{43}ex_{43} + \dot{W}_{T_{steam}} + \dot{E}x_d^{T_{steam}} \tag{28}$$

3.6. Energy and exergy efficiencies

The energy efficiency generally expresses the ratio of useful energy output to energy input, whereas the exergy efficiency generally expresses the ratio of useful exergy output to exergy input. Energy and exergy efficiency of the system and its major components are defined here.

3.6.1. Energy efficiencies

The energy efficiency of the combustion chamber is defined as

$$\eta_{cc} = \frac{\dot{m}_{18}h_{18}}{\dot{m}_{16}LHV_{mois} + \dot{m}_{17}h_{17}} \tag{29}$$

Here, the useful output is hot air and the energy inputs are moist biomass and ambient air. For the boiler, energy input is hot air from combustion chamber, and the following can be written as

$$\eta_{boiler} = \frac{\dot{m}_3h_3}{\dot{m}_{19}h_{19} + \dot{m}_2h_2} \tag{30}$$

For the ORC, the useful output work and the energy efficiency can be expressed as

$$\eta_{ORC} = \frac{\dot{W}_{T_{ORC}} + \dot{m}_{35}h_{35} - \dot{m}_{34}h_{34} + \dot{m}_{22}h_{22} - \dot{m}_{21}h_{21}}{\dot{m}_{19}h_{19} - \dot{m}_{20}h_{20}} \tag{31}$$

For the geothermal cycle, the primary energy input is geothermal energy and the secondary energy input is from organic Rankine cycle. Hence

$$\eta_{geo} = \frac{\dot{W}_{T_{steam}} + \dot{m}_{47}h_{47} - \dot{m}_{45}h_{45}}{\dot{m}_{34}h_{34} + \dot{m}_4h_4 - \dot{m}_5h_5} \tag{32}$$

An energy efficiency for the overall multi-generation system, which produces five useful outputs and has two energy inputs (geothermal and biomass), can be expressed as

$$\eta_{overall} = \frac{\dot{W}_{T_{ORC}} + \dot{W}_{T_{steam}} + \dot{Q}_e + (\dot{m}_{47}h_{47} - \dot{m}_{45}h_{45}) + (\dot{m}_{25}h_{25} - \dot{m}_{23}h_{23})}{\dot{m}_{16}LHV_{mois} + \dot{m}_{17}h_{17} + \dot{m}_{34}h_{34}} \tag{33}$$

3.6.2. Exergy efficiencies

The exergy efficiencies are defined on the same basis as energy efficiencies, but using exergy in place of energy. For the combustion chamber, physical and chemical exergy are both considered.

For combustion chamber the major exergy input is exergy of fuel. The exergy efficiency of the combustion chamber is expressible as

$$\Psi_{cc} = \frac{\dot{m}_{18}ex_{18}}{\dot{m}_{16}ex_{16} + \dot{m}_{17}ex_{17}} \tag{34}$$

The exergy efficiency of boiler can be expressed as

$$\Psi_{boiler} = \frac{\dot{m}_3ex_3}{\dot{m}_{19}ex_{19} + \dot{m}_2ex_2} \tag{35}$$

For the ORC, the useful output work and the exergy efficiency can be expressed as

$$\Psi_{ORC} = \frac{\dot{W}_{T_{ORC}} + \dot{m}_{35}ex_{35} - \dot{m}_{34}ex_{34} + \dot{m}_{22}ex_{22} - \dot{m}_{21}ex_{21}}{\dot{m}_{19}ex_{19} - \dot{m}_{20}ex_{20}} \tag{36}$$

In geothermal cycle, there are two products (electricity and hot water) and two exergy input (from geothermal and ORC), so exergy efficiency can be expressed as

$$\Psi_{geo} = \frac{\dot{W}_{T_{steam}} + \dot{m}_{45}(ex_{47} - ex_{45})}{\dot{m}_{34}ex_{34} + \dot{m}_{4}ex_{4} - \dot{m}_{5}ex_{5}} \quad (37)$$

The overall exergy efficiency of the multi-generation system having five outputs is expressed as

$$\Psi_{overall} = \frac{\dot{W}_{T_{ORC}} + \dot{W}_{T_{steam}} + \dot{E}x_{e}^{Q} + (\dot{m}_{47}ex_{47} - \dot{m}_{45}ex_{45}) + (\dot{m}_{25}ex_{25} - \dot{m}_{23}ex_{23})}{\dot{m}_{16}ex_{16} + \dot{m}_{17}ex_{17} + \dot{m}_{34}ex_{34}} \quad (38)$$

4. Results and discussion

A new multi-generation system is proposed in this study, and energy and exergy analyses are performed. The system performances are assessed of each of the five systems that are integrated to make up the multi-generation system. Parametric studies are conducted to determine the effects of variations in ambient temperature, ORC turbine input and output temperatures, and geothermal source temperature on the system power production as well as the energy and exergy efficiencies of the ORC cycle, the geothermal power cycle and the overall system. At various points in the system, numerous properties are calculated, including temperature, pressure, mass flow rate, specific enthalpy, specific entropy and specific exergy as tabulated in Table 1.

Table 1
Properties at points in the system.

State no.	Temperature (°C)	Pressure (kPa)	Mass flow rate (kg/s)	Specific enthalpy (kJ/kg)	Specific entropy (kJ/kg K)	Specific exergy (kJ/kg)
0	25	101.3	–	104.8	0.3669	0
1	85	28.09	98	140.5	0.429	12.66
2	100	2000	98	179.5	0.5273	22.36
3	400	2000	98	1241	2.57	474.9
4	335.7	28.09	98	1080	2.617	300.4
5	150	28.09	98	603.7	1.691	99.81
6	78.2	7.424	0.7998	2646	8.471	126
7	40.11	7.424	0.7998	168	0.5737	1.486
8	1.5	0.6812	0.7998	168	0.6116	−9.786
9	1.5	0.6812	0.7998	2503	9.114	−208.3
10	34	0.6812	55	90.43	0.1952	59.59
11	34	7.424	55	90.43	0.1952	59.6
12	71.64	7.424	55	166	0.4249	66.68
13	80	7.424	54.2	185.6	0.4665	73.93
14	41.36	7.424	54.2	109	0.2378	65.45
15	36.06	0.6812	54.2	109	0.2048	75.28
16	25	101.3	8	–	–	18,951
17	25	101.3	45.5	298.6	5.695	0
18	1800	101.3	53.5	2344	7.843	1476
19	1800	101.3	53.5	2344	7.843	1476
20	120	101.3	53.5	394.3	5.974	12.68
21	70	101.3	53.5	343.8	5.837	3.1
22	110	101.3	53.5	384.2	6.378	10.3
23	25	101.3	0.7	–	–	–
24	35	101.3	53.5	90.25	5.922	0.318
25	60	101.3	0.7	–	–	–
26	25	101.3	1.22	298.4	6.86	0
27	25	20,000	1.22	265.5	5.237	103.5
28	−106	20,000	1.22	63.08	4.335	169.9
29	−191.6	101.3	1.22	63.08	5.348	−131.9
30	−191.6	101.3	0.183	−121.1	3.041	371.3
31	−191.6	101.3	1.037	78.6	5.544	−175
32	25	101.3	1.037	298.6	5.695	0
33	170	500	200	–	–	–
34	170	1800	200	719.8	2.041	116.2
35	207.2	1800	200	953.4	2.541	200.7
36	151.9	500	200	953.4	2.597	183.8
37	151.9	500	29.69	2749	6.821	720.3
38	151.9	500	170.3	640.4	1.861	90.3
39	111.4	150	170.3	640.4	1.884	83.39
40	111.4	150	13.25	2693	7.223	545.4
41	111.4	150	157.1	467.2	1.434	44.42
42	45.82	10	42.94	2249	7.098	138.1
43	36.65	10	42.94	153.5	0.5273	0.8611
44	89.1	150	157.1	373.2	1.182	25.47
45	25	101.3	1000	104.8	0.3669	0
46	46.51	101.3	1000	194.8	0.6583	3.142
47	50.04	101.3	1000	209.6	0.7042	4.217

Note that the HTF (heat transfer fluid) n-octane starts decompose around 460 °C in elemental C. For the present study it is assume that temperature HTF can be maintain below 460 through special arrangement. Other HTF with high decomposition temperature can be used for simplification.

Table 2
System parameters and efficiencies obtained for the developed system.

Parameter	Value	Efficiency	Value (%)
$\dot{Q}_{gen}$	2.70 MW	η_{geo}	64.2
$\dot{Q}_{Evap}$	1.87 MW	η_{ORC}	52.2
COP_{chill}	0.69	η_{mg}	56.5
$COP_{Exchill}$	0.13	η_{sg}	11.8
COP_{Liq}	0.07	Ψ_{geo}	50.9
$\dot{W}_{T_{ORC}}$	13.4 MW	Ψ_{ORC}	42.3
$\dot{W}_{T_{steam}}$	17.6 MW	Ψ_{mg}	20.3
$\dot{W}_{Total}$	31.0 MW	Ψ_{sg}	17.3

4.1. Efficiencies and effect of multi-generation

The analysis involves the determination of the energy and exergy efficiencies for major system components, the energetic and exergetic coefficients of performance for the absorption chiller cycle and the liquefaction cycle, the work output of the ORC and steam turbines, the heat transfer to the chiller generator, and the cooling capacity of the absorber (see Table 2). The ORC energy and exergy efficiencies are found to be 52.2% and 42.3% respectively, while the energy and exergy efficiencies of the geothermal power cycle are 64.2% and 50.9% respectively. The energy efficiency of the overall system is found to be 56.5%, whereas the overall exergy efficiency is only 20.3%. The variations in system efficiencies are illustrated in Fig. 2. The energetic COP (coefficient of performance) of the chiller absorption is 0.68, while the exergetic COP is 0.13. The COP of the liquefaction cycle is shown to be 0.07. A total of 31.0 MW of power is produced by system (13.4 MW by the ORC turbine and 17.6 MW by the steam turbine).

4.2. Exergy destruction

Although it is assumed there is no heat loss to the surroundings from both the ORC and the steam turbines, both devices have exergy destructions. To determine the exergy losses for the system, the exergy destruction for all major components is calculated (see Fig. 3). The largest exergy destruction rates occur in the combustion chamber (as 72.3 MW) and the boiler (as 33.8 MW). The exergy loss rates is for Water Heater 1 (as 6.15 MW) and Water Heater 2 (as 5.18 MW) are much smaller, while the exergy destruction rates for the ORC turbine (as 3.73 MW) and the steam turbine (as 5.07 MW) are smaller still.

4.3. Parametric study results

The output of any system depends on the input parameter and operating conditions. A change in any parameter of a system generally affects its outputs and efficiency. A parametric analysis is carried out for the proposed system to determine the effect on its exergy and energy efficiencies of varying several important system parameters: ambient conditions, ORC turbine input and output temperature and geothermal source temperature.

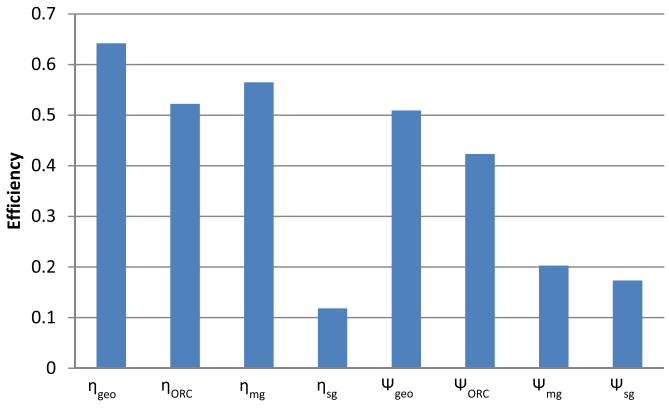

Fig. 2. Energy and exergy efficiencies for the overall system and sub-systems.

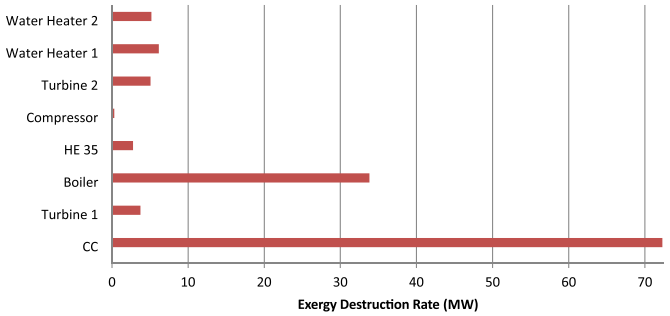

Fig. 3. Exergy destruction rates of major system components.

4.3.1. Effects of varying ambient conditions on system

Ambient conditions generally affect the performance of a system, and variations in ambient conditions can increase or decrease performance. For instance, exergy destruction rate varies directly with ambient temperature. In the current study, the ambient temperature is considered to be 298 K and the ambient pressure 101.325 kPa. To determine the effect of changes in ambient temperature on exergy destruction rate for major components in the system, the ambient temperature is varied between 288 K and 303 K. The results (see Fig. 4) show that as the ambient temperature is raised from 288 K to 303 K, the exergy destruction rate increases in combustion chamber from 71.3 MW to 72.7 MW, in the boiler from 32.8 MW to 34.3 MW, in the ORC turbine from 3.68 MW to 3.75 MW and in the steam turbine from 5.0 MW to 5.1 MW, whereas it decreases in Water Heater 1 from 8.02 MW to 3.81 MW and in Water Heater 2 from 5.88 MW to 4.91 MW.

Although the exergy destruction rates are highest for the CC (combustion chamber) and the boiler, the variations with ambient temperature of the exergy destruction rates for other system components are worth noting. A graph has been plotted excluding the boiler and the CC to more clearly show the variations in exergy destruction rates for the remaining components (see Fig. 5).

The effects of variations in ambient temperature on the energy and exergy efficiencies of the system and its components are also determined. When ambient temperature rises from 288 K to 303 K, it is observed that the system exergy efficiency increases from 20.0% to 20.4%, while system energy efficiency remains relatively

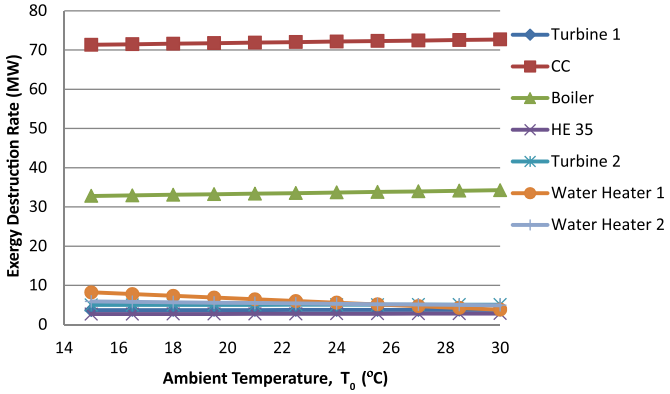

Fig. 4. Variation of exergy destruction rates of system components with ambient temperature.

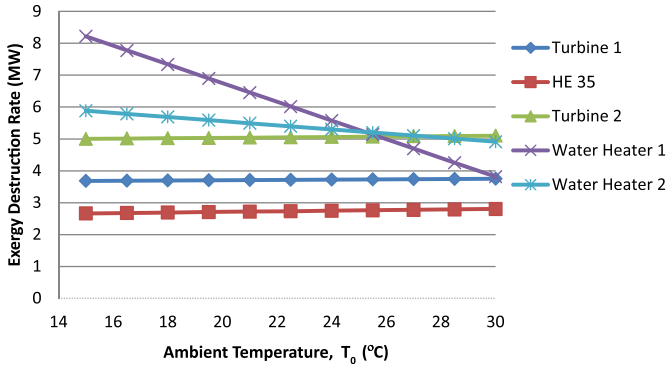

Fig. 5. Variation of exergy destruction rates of system components with ambient temperature, excluding combustion chamber and boiler.

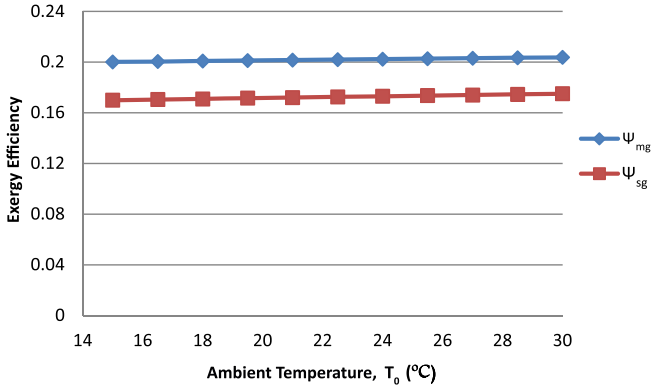

Fig. 6. Variation in system exergy efficiency with ambient temperature.

constant, as shown in Fig. 6. The variations in the exergy efficiencies of selected major system components are determined with respect to changes in ambient temperature. It is found that, as ambient temperature increases, the exergy efficiencies increase for all heat exchangers and decrease for other components (i.e., turbine, combustion chamber, boiler and dryer).

As the ambient temperature increases from 288 K to 303 K, as shown in Fig. 7, the exergy efficiency for the ORC turbine decreases from 92.5% to 91.7%, for the CC decreases from 52.9% to 51.7%, for the boiler decreases from 60.2% to 57.1%, for the dryer decreases from 6.8% to 2.4% and for the steam turbine decreases from 84.1% to 81.3%.

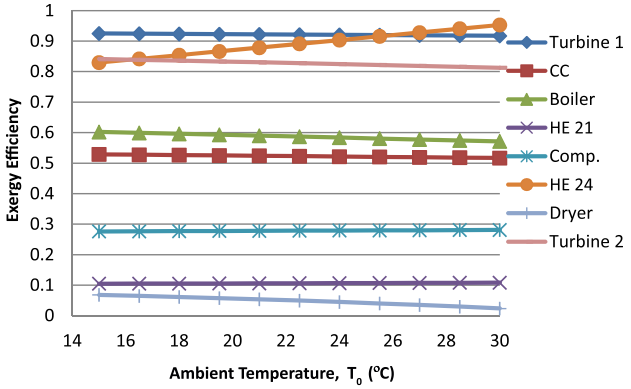

Fig. 7. Variation in exergy efficiency of major system components with ambient temperature.

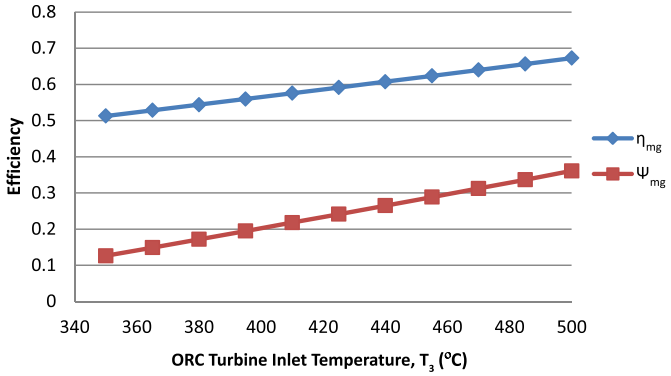

Fig. 8. Variation in system efficiencies with ORC TIT.

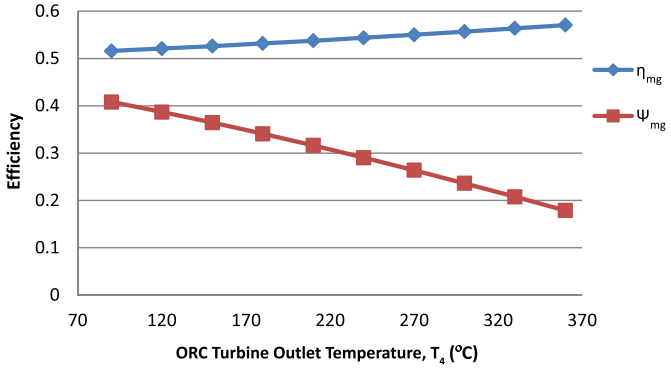

Fig. 9. Variation in system efficiencies with ORC turbine outlet temperature.

4.3.2. *Effects of ORC turbine inlet and outlet temperatures and mass flow rates on system efficiency*

The power output from a turbine generally depends on the turbine inlet and outlet temperatures and pressures. It is found that both exergy and energy efficiencies of the system increase with increasing inlet temperature to the ORC turbine (see Fig. 8). The energy efficiency of the system is observed to increase from 51.3% to 67.3%, while the exergy efficiency increases from 12.6% to 36.1%, as the TIT (turbine inlet temperature) increases from 623 K to 773 K.

The effects of turbine outlet temperature on system efficiency are also investigated. As can be seen in Fig. 9, the system energy efficiency increases from 51.6% to 57.1%, while the exergy efficiency decreases from 40.8% to 17.9%, when the turbine outlet temperature increases from 363 K to 633 K. Fig. 10 shows the effect of varying

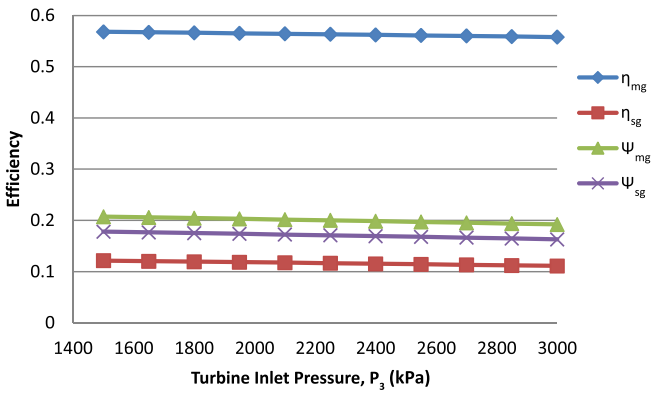

Fig. 10. Variation in system efficiencies with ORC turbine inlet pressure.

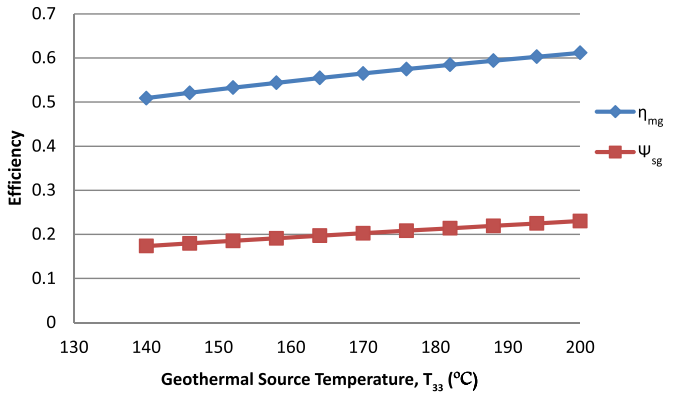

Fig. 11. Variation in system efficiencies with geothermal source temperature.

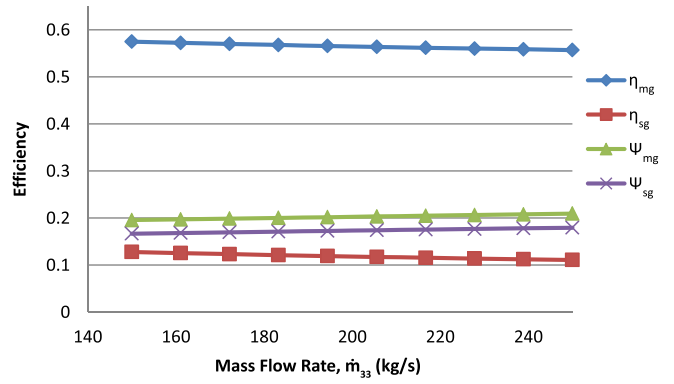

Fig. 12. Variation in system efficiencies with mass flow rate of hot water from geothermal well.

turbine inlet pressure on system efficiency. It can be seen that the effect of turbine inlet pressure on efficiency of system is not too significant since, when the turbine inlet pressure increases from 1500 kPa to 3000 kPa, the system energy efficiency decreases from 56.8% to 55.8%, whereas the system exergy efficiency decreases from 20.7% to 19.2%.

4.3.3. *Effects of geothermal source temperature and mass flow rate on system efficiency*

Geothermal water at a temperature higher than 423 K is mainly used for power production and the geothermal source temperature is taken to be 443 K in this investigation. The effect on the system's energy and exergy efficiencies of varying the geothermal source temperature is assessed here. As that parameter increases from 403 K to 473 K, the energy efficiency of the system rises from 50.9% to 61.2% and the exergy efficiency rises from 17.4% to 23.0%, with the temperature increase as illustrated in Fig. 11.

It is shown in Fig. 12 that the mass flow rate of hot water from the geothermal well strongly affects the exergy and energy efficiencies. It is observed that the exergy efficiency of the system increases with increasing mass flow rate, whereas the energy efficiency decreases.

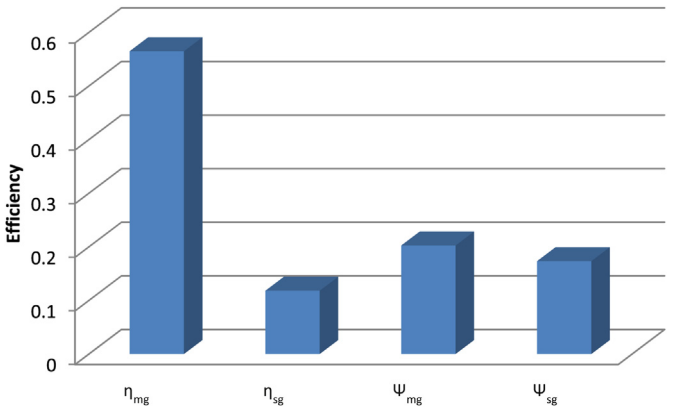

Fig. 13. Energy and exergy efficiencies of single- and multi-generation systems.

4.4. *Effects of single- and multi-generation system*

In order to determine the behaviour of a multi-generation system relative to that of a single generation system, the energy and exergy efficiencies are calculated without considering the multiple outputs like chilling effect, water heating and drying. It is found that the energy efficiency of the overall system is reduced by a significant amount in this instance, from 56.5% to 11.8% (see Fig. 13). The exergy efficiency also decreases, but less markedly, from 20.3% to 17.3%. Hence, the benefits of multi-generation in terms of additional products are important and have a significant effect on efficiencies.

5. Conclusions

A renewable energy-based multi-generation system is developed and analyzed based on the energy and exergy approaches. The overall energy and exergy efficiencies, heat losses and exergy destruction are investigated and determined, and the following main findings are obtained:

- The overall energy and exergy efficiencies of the present system become 56.5% and 20.3%, respectively.
- The energy and exergy efficiencies of the organic Rankine cycle are 52.2% and 42.3%, respectively.
- The energy and exergy efficiencies of the geothermal cycle are 64.2% and 50.9%, respectively.
- The energetic and exergetic COPs of the absorption chiller cycle are 0.69 and 0.13, respectively.
- The maximum exergy destruction rates occur in the combustion chamber as 72.3 MW and the boiler as 33.8 MW.

In summary, increasing the number of useful outputs significantly affects both energy and exergy efficiencies. The energy efficiency rises by 44.7% and the exergy efficiency by 2.9%, for the multi-generation system over a single generation system. A parametric study shows that the variations in system parameters directly influence all exergy destructions and energy and exergy efficiencies of the system and its components. The present multi-generation system also helps achieve better resource utilization.

References

[1] Murphy SH, Niitsuma SH. Strategies for compensating for higher costs of geothermal electricity with environmental benefits. Geothermics 1999;28:693–711.
[2] Gunerhan GG, Kocar G, Hepbasli A. Geothermal energy utilization in Turkey. Int J Energy Res 2001;25:769–84.
[3] Ozgener L, Hepbasli A, Dincer I. Energy and exergy analysis of salihli geothermal district heating system in Manisa, Turkey. Int J Energy Res 2005;29:393–408.
[4] Coskun C, Oktay Z, Dincer I. Modified exergoeconomic modeling of geothermal power plants. Energy 2011;36:6358–66.
[5] Cohce MK, Dincer I, Rosen MA. Energy and exergy analyses of a biomass-based hydrogen production system. Bioresour Technol 2011;102:8466–74.
[6] Filho PA, Badr O. Biomass resources for energy in north-eastern Brazil. Appl Energy 2004;77:51–67.

[7] Al-Sulaiman FA, Dincer I, Hamdullahpur F. Energy and exergy analyses of a biomass trigeneration system using an organic Rankine cycle. Energy 2012;45:975–85.
[8] Dincer I, Zamfirescu C. Renewable energy based multi-generation systems. Int J Energy Res 2012;36:1403–15.
[9] Dincer I, Zamfirescu C. Potential options to greenize energy systems. Energy Int J 2012;46:5–15.
[10] Pouria A, Dincer I, Rosen MA. Performance assessment and optimization of a novel integrated multigeneration system for residential buildings. Energy Build 2013;67:568–78.
[11] Zamfirescu C, Dincer I, Verelli T, Wagar WR. Exergy, environmental and cost analyses of low capacity concentrated solar driven heat engines for power and heat cogeneration. Int J Energy Res 2012;36:397–408.
[12] Bhattacharyya SC, Thuy N. Cogeneration potential in pulp and paper industry of Vietnam. Int J Energy Res 2005;29:345–58.
[13] Al-Sulaiman FA, Dincer I, Hamdullahpur F. Exergy analysis of an integrated solid oxide fuel cell and organic Rankine cycle for cooling, heating and power production. J Power Sources 2010;195:2346–54.
[14] Dincer I, Rosen MA, Zamfirescu C. Exergetic performance analysis of a gas turbine cycle integrated with solid oxide fuel cells. J Energy Resour Technol 2010;131:1–11.
[15] Wiegerinck GFM, Burger JF, Holland HJ, Hondebrink E, Brake ter HJM, Rogalla H. A sorption compressor with a single sorber bed for use with a Linde–Hampson cold stage. Cryogenics 2006;46:9–20.
[16] Maytal BZ. Maximizing production rates of the Linde–Hampson machine. Cryogenics 2006;46:49–54.
[17] Kanoglu M, Ali B, Ceyhun Y. Thermodynamic analysis of models used in hydrogen production by geothermal energy. Int J Hydrogen Energy 2010;35:8783–91.
[18] Thomas B, Henning S. Hybrid membrane/cryogenic separation of oxygen from air for use in the oxy-fuel process. Energy 2010;35:1884–97.
[19] Carlo C, Riccardo F, Edoardo M. Thermodynamic analysis of an organic Rankine cycle for waste heat recovery from gas turbines. Energy 2014;65:91–100.
[20] Francesco C, Claudio C, Alberto C, Laura V. Thermoeconomic analysis and off-design performance of an organic Rankine cycle powered by medium-temperature heat sources. Sol Energy 2014;103:595–609.
[21] Markus P, Florian H, Dieter B. Thermodynamic analysis of double-stage biomass fired organic Rankine cycle for micro-cogeneration. Int J Energy Res 2012;36:944–52.
[22] Srinivas J, Gupta ASSKS, Reddy BV. Parametric simulation of steam injected gas turbine combined cycle. Proc Ins Mech Eng Part A: J Power Energy 2007;221:873–82.
[23] Pouria A, Dincer I, Rosen MA. Development and assessment of an integrated biomass-based multi-generation energy system. Energy 2013;56:155–66.
[24] Basu P. Combustion and gasification in fluidized beds. Taylor & Francis Group, LLC; 2006.
[25] Szargut J, Morris DR, Steward FR. Exergy analysis of thermal, chemical, and metallurgical processes. New York: Hemisphere; 1988.
[26] Dincer I, Exergy Rosen MA. Energy, environment and sustainable development. 2d ed. Oxford, UK: Elsevier; 2013.